Analysis of the Nonlinearity of El Niño–Southern Oscillation Teleconnections*

Claudia Frauen, Dietmar Dommenget, and Nicholas Tyrrell

*School of Mathematical Sciences, and ARC Centre of Excellence for Climate System Science, Monash University,
Clayton, Victoria, Australia*

Michael Rezny

*Met Office, Exeter, United Kingdom, and ARC Centre of Excellence for Climate System Science, Monash University, Clayton,
Victoria, Australia*

Scott Wales

University of Melbourne, and ARC Centre of Excellence for Climate System Science, Melbourne, Victoria, Australia

(Manuscript received 9 December 2013, in final form 10 April 2014)

ABSTRACT

El Niño–Southern Oscillation (ENSO) has significant variations and nonlinearities in its pattern and strength. ENSO events vary in their position along the equator, with some located in the central Pacific (CP) and others in the east Pacific (EP). To study how these variations are reflected in global ENSO teleconnections, both observations and idealized atmospheric general circulation model (AGCM) simulations are analyzed. Clear nonlinearities exist in observed teleconnections of sea level pressure (SLP) and precipitation. However, it is difficult to distinguish if these are caused by the different signs, strengths, or spatial patterns of events (strong El Niño events mostly being EP events and strong La Niña events mostly being CP events) or by combinations of these. Therefore, sensitivity experiments are performed with an AGCM forced with idealized EP and CP ENSO sea surface temperature (SST) patterns with varying signs and strengths. The response is generally stronger for warm events than for cold events and the teleconnection patterns vary with changing SST anomaly patterns. EP events show stronger nonlinearities than CP events. The nonlinear responses to ENSO events can be explained as a combination of nonlinear responses to a linear ENSO (fixed pattern but varying signs and strengths) and a linear response to a nonlinear ENSO (varying patterns). Any observed event is a combination of these aspects. While in most tropical regions these add up, leading to stronger nonlinear responses than expected from the single components, in some regions they cancel each other, resulting in little overall nonlinearity. This leads to strong regional differences in ENSO teleconnections.

1. Introduction

El Niño–Southern Oscillation (ENSO) is the most important mode of interannual climate variability. It has its origin in the interaction of the tropical Pacific Ocean and the atmosphere but its teleconnections reach far beyond the tropical Pacific; for example, the tropical Indian and Atlantic Oceans and the adjacent continents are influenced by ENSO (e.g., Latif and Barnett 1995; Enfield and Mayer 1997). One typical feature of ENSO is its amplitude asymmetry. Positive events (El Niño) tend to be stronger than negative events (La Niña) (e.g., Burgers and Stephenson 1999; Kang and Kug 2002; An and Jin 2004; Frauen and Dommenget 2010). However, other studies have shown that ENSO is nonlinear not only in its amplitude but also in its spatial pattern (e.g., Hoerling et al. 1997; Takahashi et al. 2011; Yu and Kim 2011; Choi et al. 2012) and time evolution (e.g., Larkin and Harrison 2002; Ohba and Ueda 2009; Okumura and Deser 2010). Dommenget et al. (2013) showed that significant differences exist in the patterns between positive and negative events and between strong and weak events, which mostly describes the differences between central

and eastern Pacific events. Several studies also pointed out that differences exist in the global teleconnections of central and eastern Pacific events. Ashok et al. (2007) show that, depending on the season, the impacts of the central Pacific El Niño on specific regions can be opposite to those of the eastern Pacific El Niño. Also, Hu et al. (2012) show that besides the tropics especially the eastern Pacific, North America, and the North Atlantic have robust climate differences between the eastern and central Pacific El Niño events. Other studies pointed out significant differences in the regional impact of central and eastern Pacific El Niño events over, for example, East Asia (Yuan and Yang 2012), the North Pacific, the southwestern United States (Zhang et al. 2012), Australia (Taschetto and England 2009), and Europe (Graf and Zanchettin 2012).

Previous studies have also shown that the responses to El Niño and La Niña events are not simply opposite. Significant nonlinearities exist in the global precipitation and sea level pressure (SLP) responses. Nonlinearities in the tropical Pacific precipitation response are to be expected. The sea surface temperature (SST) threshold for deep convection (e.g., Gadgil et al. 1984) means that there is a much stronger response to warm SST anomalies than to cold ones. The large zonal climatological SST gradient across the Pacific also results in a spatial shift in the rainfall response between El Niño and La Niña events because, in general, convection responds to the absolute rather than the anomalous SST (Hoerling et al. 1997). Hoerling et al. (2001) also showed that nonlinearities in the tropical precipitation response as well as in the extratropical atmospheric response mainly emerge for stronger events. Chung et al. (2014) and Power et al. (2013) demonstrated that global warming can intensify the nonlinear tropical precipitation response for El Niño events. Also regional rainfall responses, as for example shown by Power et al. (2006) for Australia and over the western United States and northern Mexico, by Cai et al. (2010) for eastern Australia, and by Smith et al. (2013) for the New Guinea region, show significant nonlinear relationships with ENSO. The nonlinear response in extratropical SLP, however, cannot simply be explained by shifts in the deep convection between El Niño and La Niña events (Larkin and Harrison 2002).

This study will systematically show how differences in the sign, amplitude, and pattern of tropical Pacific SST anomalies are reflected in global SLP and precipitation responses. This is achieved by analyzing sensitivity experiments, in which an atmospheric general circulation model (GCM) is forced with idealized ENSO SST patterns of varying sign and strength. Here, we will focus our analysis on annual mean responses and will not consider

seasonal differences, although considerable seasonal variations do exist in these characteristics. Because of the limited space of this study, we will leave analyses of seasonal differences for later studies.

The remainder of this article is organized as follows. In section 2 we describe the data and model simulations used for this study. The nonlinearities in observed ENSO teleconnections are analyzed in section 3. In section 4 we study the ENSO teleconnections in an atmospheric GCM forced with idealized ENSO SST patterns. Finally, the main findings and outcomes of this study are summarized in section 5.

2. Data and models

For the analyses of observed ENSO teleconnection nonlinearities in this study linearly detrended monthly mean SST anomalies for the period 1950–2010 are calculated from the Hadley Centre Global Sea Ice and Sea Surface Temperature dataset (HadISST; Rayner et al. 2003). The same is done for SLP data based on the National Centers for Environmental Prediction (NCEP) reanalysis dataset (Kalnay et al. 1996) for the same period and for precipitation data based on the Global Precipitation Climatology Project (GPCP) version 2 monthly satellite-gauge data for the period 1979–2010 (Adler et al. 2003).

A series of sensitivity experiments with a full complexity atmospheric GCM forced with idealized SSTs in the tropical Pacific (30°S–30°N, 120°E–70°W) were carried out to further support the limited statistics from the relatively short period of observations and to better understand the interactions. The atmospheric model used in this study is a low-resolution version (3.75° × 2.5°) of the atmospheric component of the Australian Community Climate and Earth System Simulator (ACCESS) model (Bi et al. 2013), which is the Met Office (UKMO) Unified Model atmospheric GCM with Hadley Centre Global Environment Model version 2 (HadGEM2) physics (Davies et al. 2005; Martin et al. 2010; Martin et al. 2011). Outside the tropical Pacific the atmospheric model is coupled to a simple slab ocean model (Washington and Meehl 1984; Dommenget and Latif 2002; Murphy et al. 2004; Dommenget 2010). A flux correction scheme is applied here to force the model SSTs to closely follow the prescribed HadISST SST climatology. However, the SSTs are still able to respond to forcings from the tropical Pacific. This model will be referred to as ACCESS-slab. A 100-yr control simulation with prescribed climatological SSTs in the tropical Pacific is performed with this model. Additionally, 12 sensitivity experiments are performed with prescribed ENSO patterns in the tropical Pacific. To analyze the models ability
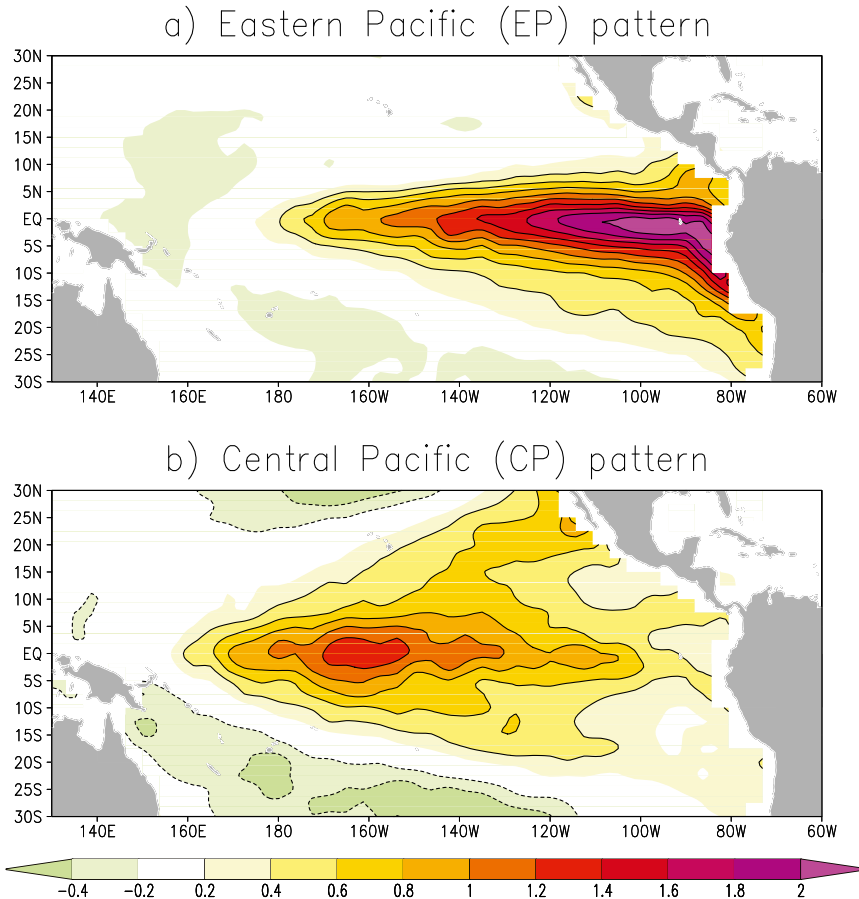
a) Eastern Pacific (EP) pattern

b) Central Pacific (CP) pattern

FIG. 1. Standardized ENSO patterns used for the sensitivity experiments based on the rotated EOF patterns after Dommenget et al. (2013) normalized by their Niño-3.4 SST anomalies [K (K Niño-3.4)$^{-1}$]: (a) eastern Pacific (EP) pattern and (b) central Pacific (CP) pattern.

to correctly simulate the SLP and precipitation teleconnections a further simulation is performed, in which the atmospheric model is forced with the monthly HadISST SSTs from 1950 to 2010. This simulation will be referred to as ACCESS-AMIP (referring to the Atmospheric Model Intercomparison Project).

The prescribed ENSO patterns (see Fig. 1) are based on the idealized El Niño (PC$_{El-Niño}$) and La Niña (PC$_{La-Niña}$) patterns defined in Dommenget et al. (2013) (see also their Fig. 4). Their PC$_{El-Niño}$ and PC$_{La-Niña}$ are an orthogonal rotation of the first and second principal components (PCs) of tropical Pacific SST and describe the nonlinear spatial structure of ENSO in an optimal way motivated by the scatterplot between PC1 and PC2 [see Fig. 2 herein and also Fig. 3 in Dommenget et al. (2013) for time series of PC1 and PC2]. The scatter points do not form an isotropic cloud, as expected for linear interactions, but appear to have two main orthogonal directions (PC$_{El-Niño}$ and PC$_{La-Niña}$), which was also found by Takahashi et al. (2011). It can be seen that

strong El Niño events (large positive values of PC1) are associated with positive values of PC2. A superposition of PC1 + PC2 leads to the typical eastern Pacific (EP) pattern superimposed in the upper right quadrant. This defines PC$_{El-Niño}$. The EP pattern is narrower around the equator and has its maximum directly off the coast of South America. Strong La Niña events (large negative values in PC1) are also associated with positive values of PC2. Thus, a superposition of −PC1 + PC2 leads to the typical central Pacific (CP) pattern (upper left quadrant), which is meridionally wider and has its maximum in the central Pacific. This defines PC$_{La-Niña}$. Weak El Niño and La Niña events have mostly negative values in PC2. This means that a weak El Niño (La Niña) event has the same pattern as a strong La Niña (El Niño) event with opposite sign. The two patterns, EP (PC$_{El-Niño}$) and CP (PC$_{La-Niña}$), are therefore optimal to study the teleconnections of ENSO.

For the sensitivity experiments these two different patterns were normalized to have a Niño-3.4 (5°S–5°N,
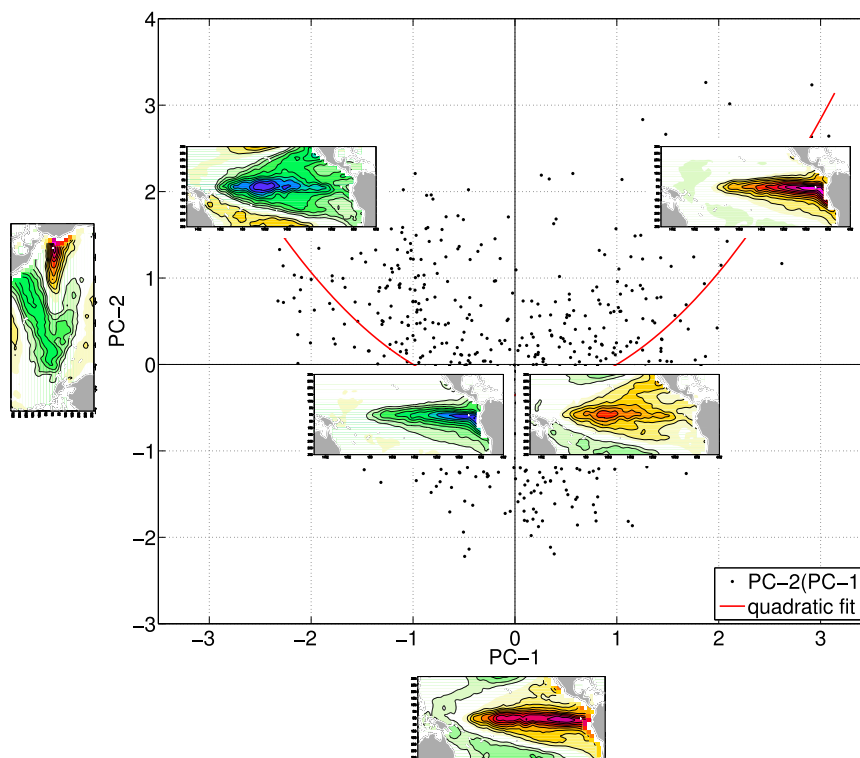
FIG. 2. Scatterplot of observed tropical Pacific SST anomalies PC1 and PC2 data pairs (black dots) with a quadratic fit (red line) after Dommenget et al. (2013). Superimposed are the typical SST anomaly patterns relating to the different regimes. Next to the axes are the EOF patterns associated with the respective PCs.

120°–170°W) mean SST anomaly of +1 K and added to the HadISST climatology in the tropical Pacific with positive and negative signs: Positive eastern Pacific (EP+), negative eastern Pacific (EP−), positive central Pacific (CP+), and negative central Pacific (CP−). The patterns were added with different strengths: 50%, 100%, and 200%, corresponding to the normalized patterns multiplied with 0.5, 1, and 2. To get statistically significant results the experiments were run for different periods of time. An overview of the experiments can be seen in Table 1.

3. Observed ENSO teleconnections

Before we go into the analysis of the nonlinearity in the ENSO teleconnections it is instructive to first look at the nonlinearities in the distribution of the climate variability itself (see Fig. 3). This will give us a first idea of what we should expect for the nonlinearities in the ENSO teleconnections. Here, we will focus on the skewness of the distribution as a zero-order estimate of nonlinearities, but later we will define nonlinearities as any deviation from a linear function.

The distribution of SST anomalies in the tropical Pacific is positively skewed in the east and negatively skewed in

the west (Fig. 3a), consistent with Burgers and Stephenson (1999). For the tropical Pacific SLP (Fig. 3b) we find roughly the opposite of the SST skewness, as SST and SLP are strongly linked to each other with opposite signs. However, the relative and absolute strength of the SLP skewness is somewhat different from that of the SST. Overall, the SLP skewness in the tropical Pacific is weaker than for SST, but stronger for many other regions outside the tropical Pacific (e.g., Indian Ocean or northern extratropics). The SLP skewness is also more pronounced in the western part of the tropical Pacific than in the eastern part, which is the opposite for the SST distribution.

TABLE 1. Overview of simulations performed: Niño-3.4 SST anomaly of the prescribed patterns and lengths of the simulations.

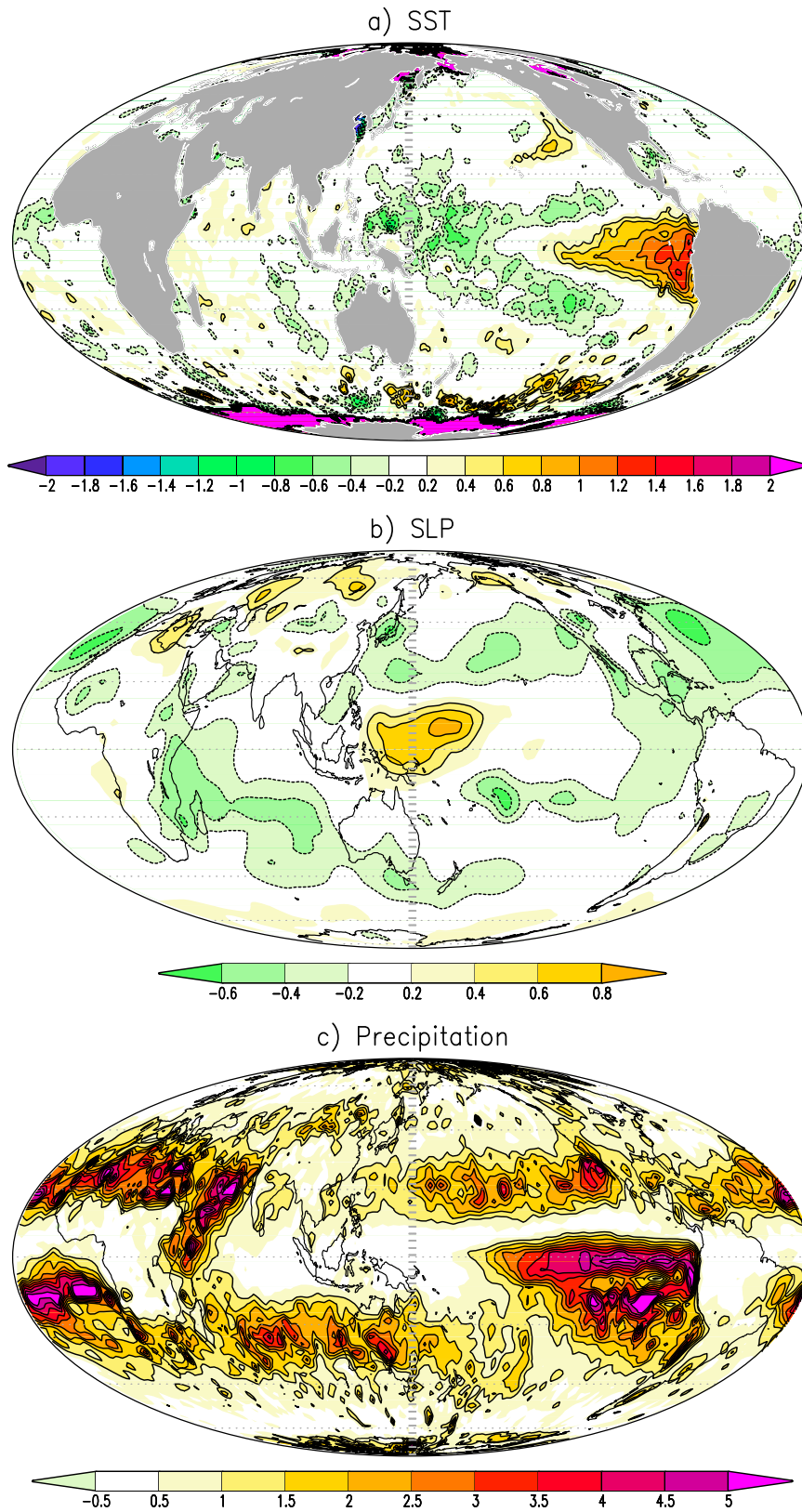|	EP	CP
200%	2.0 K (50 yr)	2.0 K (50 yr)
100%	1.0 K (100 yr)	1.0 K (100 yr)
50%	0.5 K (200 yr)	0.5 K (200 yr)
Control	0.0 K (100 yr)	
−50%	−0.5 K (200 yr)	−0.5 K (200 yr)
−100%	−1.0 K (100 yr)	−1.0 K (100 yr)
−200%	−2.0 K (50 yr)	−2.0 K (50 yr)

FIG. 3. Skewness of observed monthly mean (a) SST anomalies, (b) SLP anomalies, and (c) precipitation anomalies. Note the different color bar for precipitation.
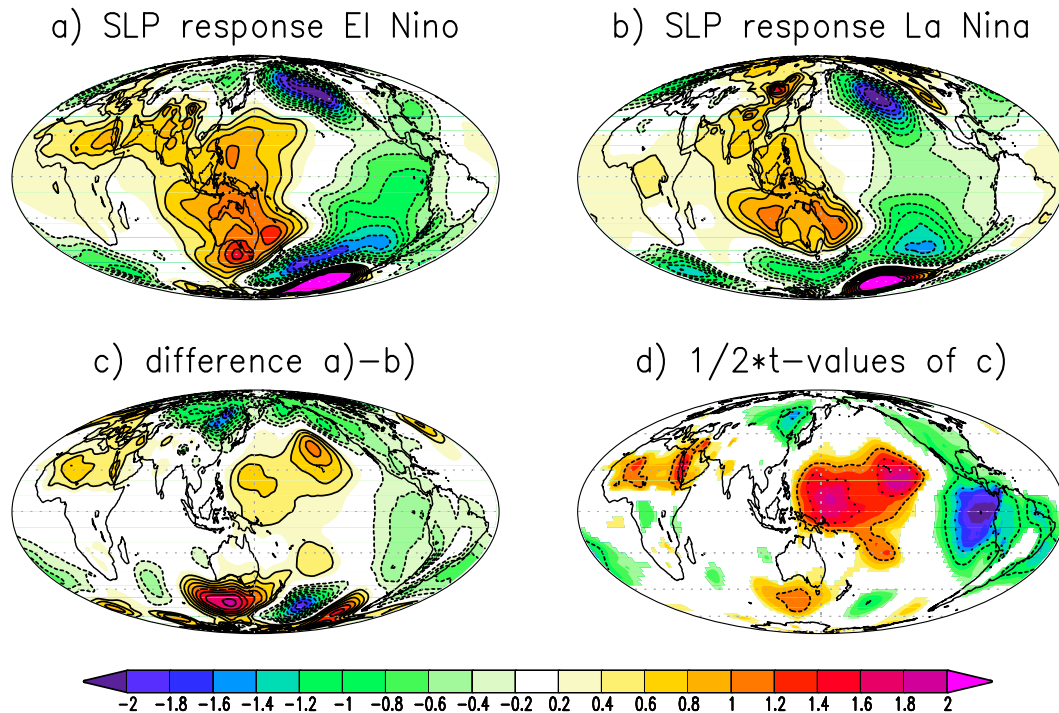
FIG. 4. Composites of observed mean SLP anomalies during (a) El Niño events and (b) La Niña events normalized by the Niño-3.4 SST anomalies (hPa K^{-1}). El Niño (La Niña) events are defined as months with PC$_{\text{El-Niño}} \geq$ 1.0 (PC$_{\text{La-Niña}} \leq -1.0$). (c) The difference between the response patterns in (a) and (b) is shown. (d) The Student's t values for the difference in (c) scaled by the factor $\frac{1}{2}$. The dashed and dotted black lines indicate the 95% and 99% confidence levels, respectively.

Precipitation has positive skewness nearly everywhere, as is well known and expected from a positive definite variable (Fig. 3c). In particular, regions with relative small mean precipitation near regions of relative strong mean precipitation [e.g., the boundaries of the intertropical convergence zone (ITCZ)] show very large values of skewness. Regions with large mean precipitation (e.g., ITCZ) show relatively small skewness. In summary, we expect the SLP to somewhat follow the SST nonlinearities, but possibly also to show some deviations from it. The precipitation teleconnections are likely to be positively skewed no matter what the SST forcing looks like. Thus, nonlinearities in precipitation may not necessarily reflect nonlinearities in ENSO teleconnections.

We base the nonlinearity of the observed ENSO teleconnections on composites of El Niño and La Niña events according to the PC$_{\text{El-Niño}}$ and PC$_{\text{La-Niña}}$ time series. All months with PC$_{\text{El-Niño}} \geq 1.0$ are classified as El Niño months and all months with PC$_{\text{La-Niña}} \leq -1.0$ are classified as La Niña events. Figure 4 shows the normalized SLP response to El Niño and La Niña events and the difference in the response patterns. The normalization by the mean Niño-3.4 SST values allows us to directly compare the composites of El Niño and La Niña events, as it

gives us the SLP response per Niño-3.4 SST anomaly. Note that the La Niña composites have reversed signs as they are normalized by the mean negative SST anomalies in the Niño-3.4 region. For a linear response model just depending on the Niño-3.4 SST anomalies both composites should be identical in this presentation.

First of all, we note that the SLP response patterns (Figs. 4a,b) have the well-known structure with the typical pattern of the Southern Oscillation and a negative SLP response over the North Pacific for positive SST anomalies in Niño-3.4. However, we can also note that the composites of El Niño and La Niña are not identical, which is quantified by the difference between these in Fig. 4c. The t values for a Student's t test of the differences as a measure of significance are shown in Fig. 4d. Positive values can result from a combination of differences: the SLP response is, for instance, stronger in amplitude per Niño-3.4 SST anomaly during El Niño events in regions where the El Niño SLP response is positive (e.g., the western tropical Pacific) or the El Niño SLP response is weaker in amplitude per Niño-3.4 SST anomaly during El Niño events in regions where the El Niño SLP response is negative (e.g., from the central Pacific to Hawaii). The converse applies for negative difference values (e.g.,
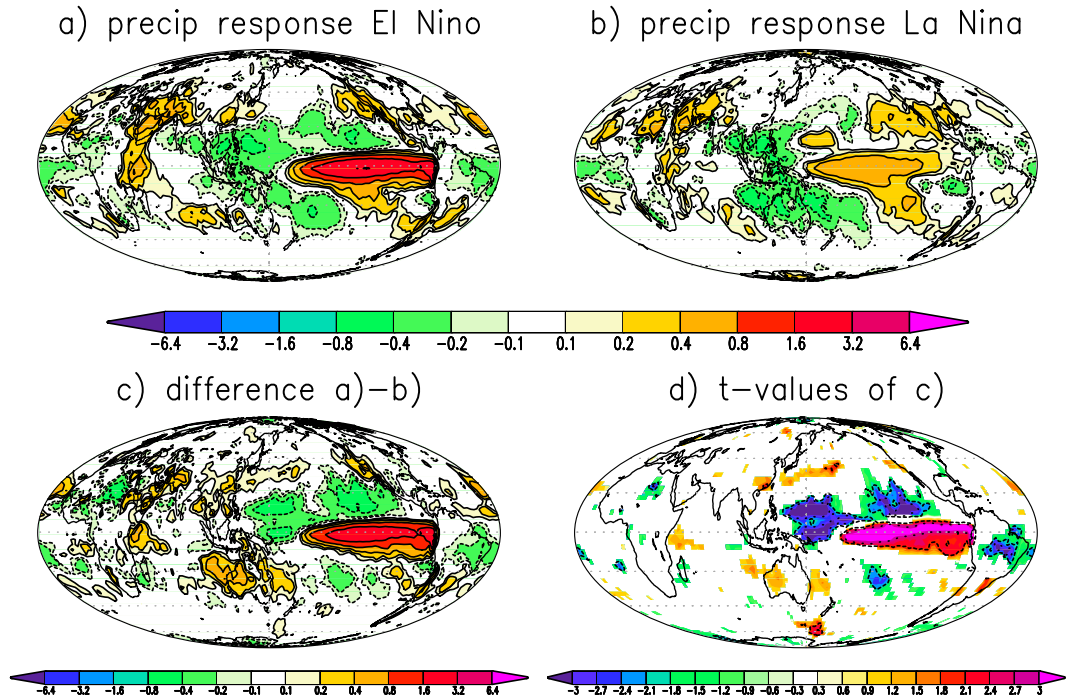
FIG. 5. As in Fig. 4, but for observed mean precipitation anomalies per climatological precipitation (value of 0.5 means the precipitation anomaly is 50% of the climatological precipitation) normalized by the Niño-3.4 SST anomalies (% K^{-1}). Please note the nonlinear color bar for (a)–(c).

eastern tropical Pacific). However, there are also combinations in which the normalized SLP responses change sign in the composites of El Niño and La Niña (e.g., northeast Asia) and where the SLP response is the same for both El Niño and La Niña events. In these cases the differences do not reflect weaker or stronger responses.

Significant nonlinearities can be found over the eastern and western tropical Pacific, the tropical to subtropical North Pacific, and the South Pacific around 30°S due to the La Niña SLP response being shifted farther to the west. Also, south of Australia a significant nonlinearity is found due to the positive La Niña SLP response here extending all the way into the Indian Ocean. Over northeast Asia we find a negative SLP response to both El Niño and La Niña, which makes it highly nonlinear. Over North Africa, South America, and the central South Pacific strong nonlinearities are found as well. However, they are not statistically significant. It is interesting to note that the Niño-3 region more or less marks the transition zone between positive and negative deviations from a linear response. The differences in the composites of El Niño and La Niña events have strong similarities with the composite of El Niño events. This suggests that the nonlinearities are, to zero or first order, reflecting a stronger response to El Niño events than to La Niña events. But, as pointed out above, some regions also show significant shifts in the response.

Figure 5 shows the mean precipitation response in percentage of the climatological precipitation. The strongest response in precipitation during an El Niño event is found over the equatorial Pacific east of the date line. During a La Niña event the response in the equatorial Pacific is weaker and the maximum is shifted farther to the west while in the far eastern equatorial Pacific only a very small response is found. In the case of an El Niño event one can also find responses in the central to western Pacific north and south of the equator and over the Maritime Continent. In the La Niña case the response south of the equator extends farther to the west over the whole of Australia and into the Indian Ocean. Other regions, which show an indication of a nonlinear response, are North Africa and Brazil. Again, outside the tropical Pacific the differences between the El Niño and La Niña responses are rarely statistically significant. Similar to the SLP response, the differences in the precipitation response look similar to the composite of El Niño events, again suggesting that the nonlinearities are to first order reflecting a stronger response to El Niño events than to La Niña events. Here, only the annual mean precipitation response is shown although precipitation has strong seasonal variations and therefore also the ENSO responses vary with seasons. However, for a seasonal analysis of the nonlinearities too few data are available.

Based on the observed ENSO response composites we highlight the following findings:

- Significant nonlinearities are found in the SLP response in the far eastern and western tropical Pacific, in the northern tropical to subtropical Pacific, south of Australia, and over northeast Asia.
- Most of the nonlinearities suggest a stronger response to El Niño events than to La Niña events, but some significant shifts in the response pattern also exist.
- For precipitation, significant nonlinearities are almost exclusively found in the tropical Pacific.
- The SLP response shows almost no nonlinearity over the Niño-3 and Niño-4 regions, where the strongest ENSO SST anomalies occur.

The observed differences between strong El Niño and strong La Niña events may result from several different factors, including the differences in the sign of the events, the differences in the strength of the events, and the differences in the pattern of the events. To separate the responses according to these different factors the database of observed events is just too small to get statistically significant results. It also needs to be noted that most observed events may be a combination of different patterns, strengths, or signs. Therefore, an analysis of idealized model simulations is necessary, in which we can separate the different aspects.

4. Sensitivity experiments

A good way to study the impacts of the different factors (sign, strength, and pattern of the events) on ENSO teleconnections is to perform sensitivity experiments with an atmospheric GCM forced by standardized ENSO patterns. An overview of the experiments performed for this study was given in section 2 and in Table 1. In the following, we will analyze how well the model performs in simulating the ENSO teleconnections in SLP and rainfall and what influence different patterns, signs, and strengths of the ENSO events have on the nonlinearities in the responses in SLP and precipitation. For precipitation we have to keep in mind that first, we only have a very limited amount of reliable observational data and second, it is well known that most of the state-of-the-art coupled climate models have strong biases in the simulated tropical precipitation (Lin 2007). However, since ENSO-related precipitation has very strong socioeconomic impacts, it is worth also analyzing the nonlinearities in ENSO teleconnections regarding precipitation.

a. Comparison with observations

To assess the model's ability in simulating the ENSO teleconnections we first take a look at the SST anomalies

in the model compared to observations. Figures 6a and 6b show composites of observed SST anomalies during El Niño and La Niña events. Figures 6c and 6d show the mean SST anomalies in the 100% EP+ and CP− experiments, which are the sensitivity experiments that are closest to the composite of the observed ENSO events (Figs. 4 and 5) although the composite threshold of $PC_{El-Niño} \geq 1.0$ or $PC_{La-Niña} \leq -1.0$ does not necessarily exclude CP+ and EP− events, respectively. We can see that even though the ocean is just represented in form of a simple slab ocean model a lot of the SST responses outside the tropical Pacific can be reproduced. However, in some regions (e.g., the eastern Indian Ocean in the EP+ case) the model produces a slightly stronger response than observed. Next, we can take a look at the ACCESS-AMIP simulation, in which the atmospheric model was forced with observed SSTs. The same composite analysis as shown for observations in Figs. 4 and 5 was performed for the SLP and precipitation anomalies obtained from the ACCESS-AMIP simulation (see Figs. S1 and S2 in the supplementary material). The SLP response patterns show good agreement with the observations, especially in the tropical Pacific. The simulated and observed El Niño composite, La Niña composite, and difference patterns show spatial correlations of above 0.85 in the tropical Pacific (30°S–30°N, 130°E–70°W). Globally between 60°N and 60°S the spatial correlations are above 0.7 for the composite patterns but only 0.47 for the difference pattern. This is mostly due to the model failing to reproduce a sufficiently strong SLP response over the Indian Ocean in the El Niño case but producing a too strong SLP response in the western Indian Ocean in the La Niña case. Also for precipitation the modeled and observed response patterns agree well in the tropical Pacific, where the strongest response is found. The spatial correlation values are above 0.89 for the El Niño composite and the difference patterns. For the La Niña composite the spatial correlation is only 0.74, which is mostly due to the precipitation response over Australia having the wrong sign. Globally between 60°N and 60°S the spatial correlation values are 0.82 for the El Niño composite, 0.55 for the La Niña composite, and 0.71 for the difference patterns.

The observed ENSO events are in general a combination of different patterns, signs, and strengths. If we compare the 100% EP+ and CP− SLP and precipitation responses (Figs. 7 and 8) with the observed, we see that also the ACCESS-slab model is able to simulate comparable response patterns, especially in the tropical Pacific. Positive forcings result in a negative SLP anomaly in the eastern tropical Pacific and a positive anomaly over the western tropical Pacific and the Maritime Continent, which represent the Southern Oscillation (Figs. 7a,d). Also, the model reproduces the observed negative
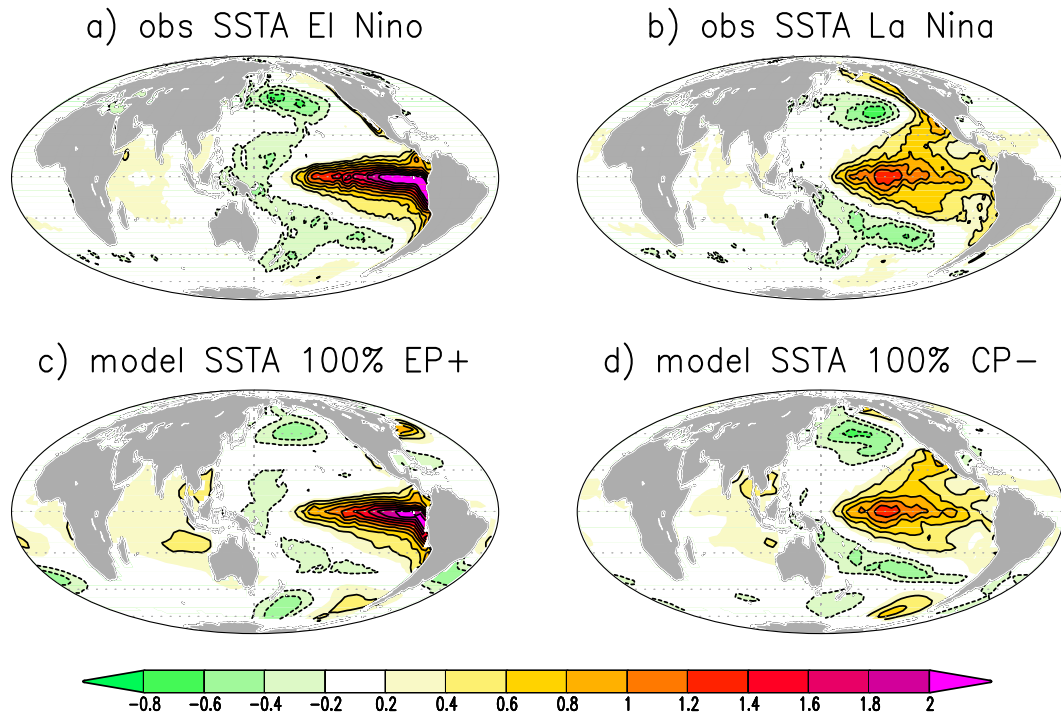
FIG. 6. (a) Composite of observed mean SST anomalies during El Niño events normalized by the Niño-3.4 SST anomalies [K (K Niño-3.4)$^{-1}$]. (b) As in (a), but for La Niña events. (c) Mean SST anomalies in the 100% EP+ simulation normalized by the Niño-3.4 SST anomalies [K (K Niño-3.4)$^{-1}$]. (d) As in (c), but for the 100% CP− simulation.

anomalies in the North and South Pacific in case of an El Niño event as well as the negative anomalies over South America and the positive anomalies over Australia. The negative CP− forcing (Fig. 7e) again reproduces the Southern Oscillation with a positive anomaly over the eastern Pacific and a negative anomaly over the western Pacific and again the response is shifted farther to the west (note again that the responses for negative forcings in Fig. 7 are shown with reversed signs because of the normalization). The strongest anomalies are found off the coast of Australia as in observations. Also, the observed positive anomalies in the North and South Pacific are simulated in the model. What the model does not capture are the responses over Africa, where the experiments either show no response (CP−) or a response with the wrong sign (EP+). Figure 7i shows the differences between the EP+ and the CP− forcing and thus shows the differences between typical strong El Niño and strong La Niña events (cf. Fig. 4c). The model captures most of the nonlinearities also found in the observations. However, the nonlinearity over northeast Asia and North Africa and the strength of the nonlinearity south of Australia are not captured.

For precipitation we find a strong increase along the equatorial Pacific and reduced precipitation over the Maritime Continent and the western to central Pacific north and south of the equator in response to positive forcings (Figs. 8a,d). In case of the EP+ forcing the negative precipitation response north of the equator extends all the way to the eastern Pacific. This is in good agreement with observations although the positive precipitation response extends too far to the west. In response to negative forcings (Figs. 8b,e) we find a reduction in rainfall along the equatorial Pacific, which is weaker than the response to positive forcings. In the CP− case we find a strong increase in precipitation over the Maritime Continent, northeast Australia, and the western to central Pacific north and south of the equator. Again, this is in good agreement with observations. The model also simulates realistic responses along the coast of California and Mexico. However, the model mostly fails to reproduce a realistic response over Australia. In the CP− case, which represents a typical La Niña event, the negative response is only found over the northeast of Australia and in the EP+ case an unrealistically strong positive response is found over western Australia. The differences between El Niño and La Niña events (Fig. 5c) are again represented by the differences between the EP+ and the CP− forcing (Fig. 8i). In the tropical Pacific region the model is mostly able to reproduce the observed
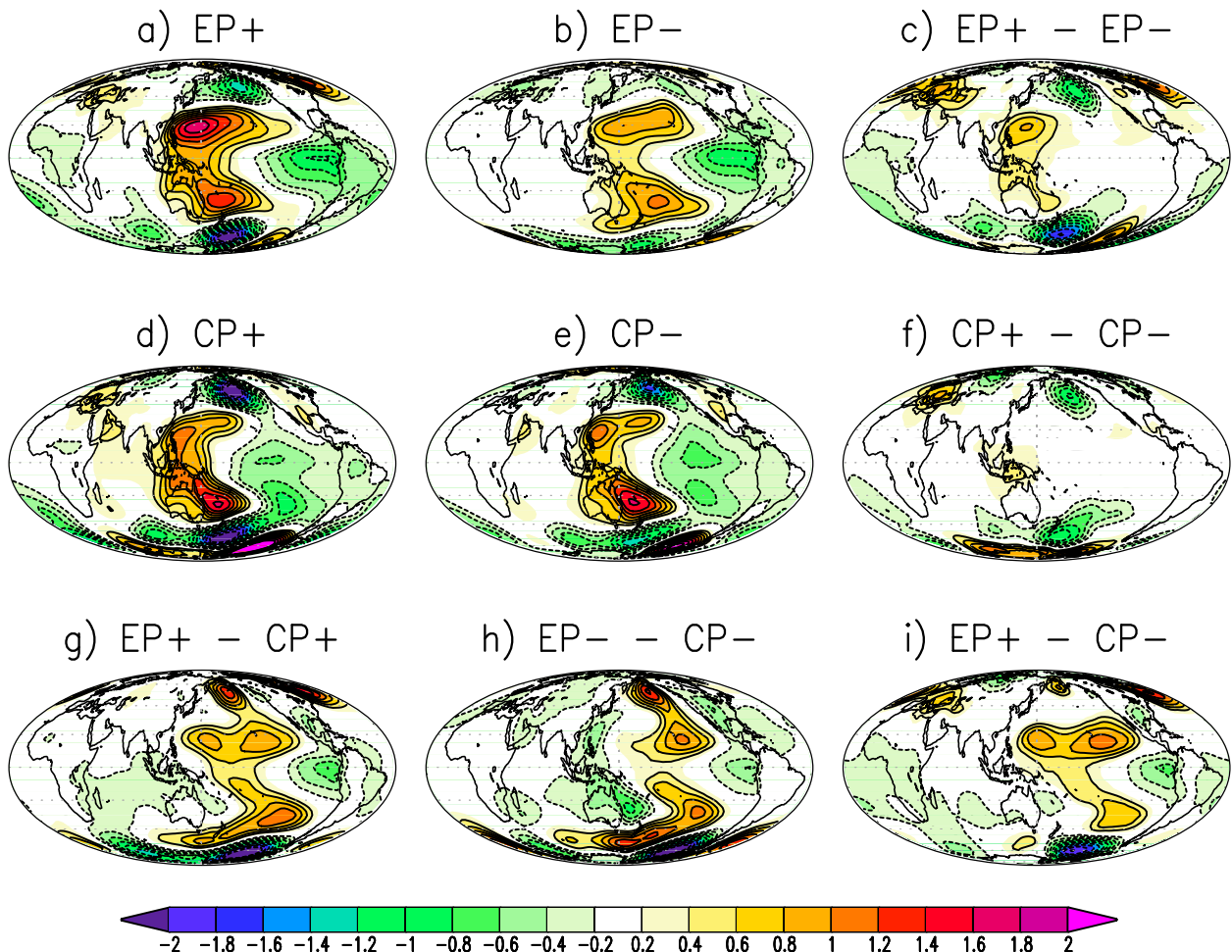
FIG. 7. SLP response patterns from the (a) EP+ 100%, (b) EP− 100%, (d) CP+ 100%, and (e) CP− 100% experiments normalized by the Niño-3.4 SST anomalies (hPa K^{-1}). Further, the differences between (c) EP+ and EP−, (f) CP+ and CP−, (g) EP+ and CP+, (h) EP− and CP−, and (i) EP+ and CP−. All differences are statistically significant at 90% level following a Student's t test.

differences. However, over Africa the model simulates significant nonlinearities, which are not observed.

Based on the ACCESS-AMIP simulation it can be concluded that the atmospheric model is able to simulate the responses in SLP and precipitation fairly well, especially over the Pacific Ocean. The comparison of the 100% sensitivity experiments with the observations also lead to the conclusion that the ACCESS-slab model appears to be a good tool to study the nonlinearities in these SLP and precipitation responses.

b. Differences due to EP and CP forcing patterns

The influence of the different forcing patterns, EP and CP, can be estimated by analyzing the differences in the response for the sensitivity experiments with the same sign of forcing and the same strength in the forcing. This is shown in Figs. 7g and 7h for SLP and Figs. 8g and 8h for precipitation. The results show that the patterns of

the forcings in the tropical Pacific have strong influences on the SLP response over most of the globe. The CP forcing has a much stronger influence over the North and South Pacific for both positive and negative forcings. Also, a small positive response is found over the Indian Ocean only for the CP forcings, especially with positive sign. The main structure may largely be characterized as a westward shift in the tropics for a CP forcing relative to the EP forcing. Thus, the CP forcing has stronger influence on the western tropical Pacific and the Indian Ocean and the EP forcing has a stronger impact on the eastern Pacific and the American continents. The extratropical responses seem to somewhat follow this westward shift characteristics, but the structure is not as clear.

Even stronger differences in the responses to EP and CP forcings are found for precipitation (Fig. 8). Especially for positive forcings a much stronger response is found in the Pacific along the equator and north of the

a) EP+   b) EP−   c) EP+ − EP−

d) CP+   e) CP−   f) CP+ − CP−

g) EP− − CP+   h) EP− − CP−   i) EP+ − CP−

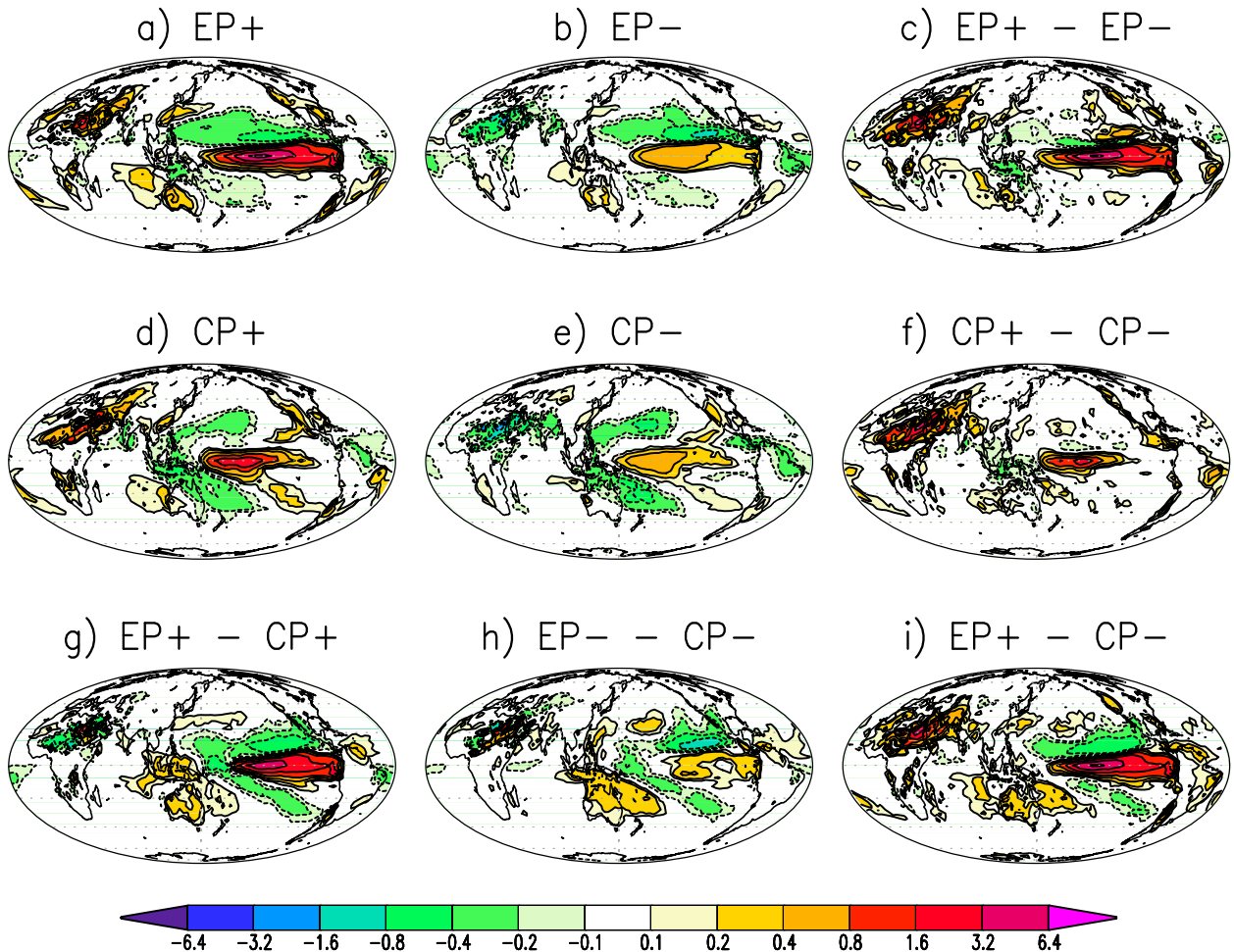| −6.4 | −3.2 | −1.6 | −0.8 | −0.4 | −0.2 | −0.1 | 0.1 | 0.2 | 0.4 | 0.8 | 1.6 | 3.2 | 6.4 |

FIG. 8. As in Fig. 7, but for mean precipitation anomalies per climatological precipitation. Again the responses are normalized by the Niño-3.4 SST anomalies (hPa K^{-1}).

equator for EP forcings. For the CP+ forcing no rainfall response is found over the far eastern equatorial Pacific. On the other hand, CP events have a much stronger influence on the Pacific south of the equator. A band of enhanced (reduced) precipitation extends from the central equatorial Pacific to the southeast Pacific for positive (negative) events. The strength of the differences between EP and CP forcings, however, also depends strongly on the sign of the forcings. Again, the main large-scale structure is a westward shift in the tropics for a CP forcing relative to the EP forcing. The extratropical response, however, does not appear to have a simple westward shift following the change in forcing pattern.

c. *Differences due to the forcing strengths and signs*

Figures 7c and 7f show the differences between the SLP responses to positive and negative forcings. In both cases the difference pattern is similar to the positive (El Niño) forcing responses, which suggests stronger responses to positive forcings than to negative forcings over most regions. The differences are mostly stronger for the EP pattern than for the CP pattern. For precipitation (Figs. 8c,f) the response to positive forcing is much stronger than the response to negative forcing over the equatorial Pacific, as was expected. Again, the difference is stronger for EP forcings.

Figure 9 shows the different SLP responses to different strengths and signs of forcings. The EP and CP −200% experiments represent the cases where the mean SSTs are the coldest and the +200% experiments where they are the warmest. Thus, the experiments in this figure are organized by coldest (bottom) to warmest (top). Again, as all responses are normalized by the Niño-3.4 SST anomalies, a linear response should result in all responses being the same. To first order, we can note that for both EP and CP forcing the strength of the response increases with the overall warming of the SST. In particular, the SLP response in the North Pacific in the EP+ case is highly
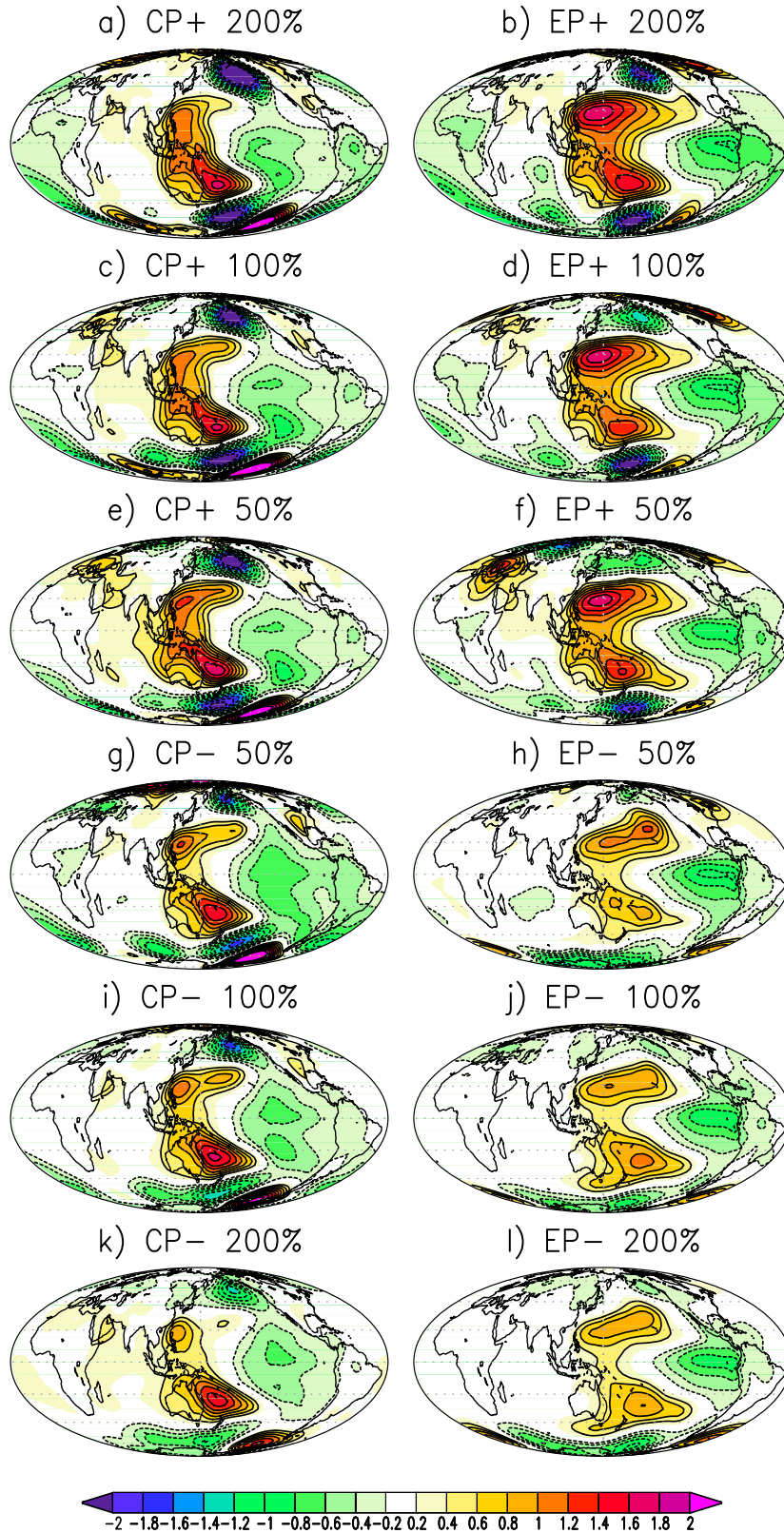
FIG. 9. SLP response patterns for the (a) CP+ 200%, (b) EP+ 200%, (c) CP+ 100%, (d) EP+ 100%, (e) CP+ 50%, (f) EP+ 50%, (g) CP− 50%, (h) EP− 50%, (i) CP− 100%, (j) EP− 100%, (k) CP− 200%, and (l) EP− 200% experiments normalized by the Niño-3.4 SST anomalies (hPa K^{-1}).

nonlinear. This result is in good agreement with Hoerling et al. (2001), who found a stronger wintertime atmospheric circulation response over the North Pacific for El Niño than for La Niña events, which was only evident for strong events.

This general result of increasing responses with increasing anomalies suggests that a warmer background state will in general lead to a stronger atmospheric response for the same SST anomalies. If we for instance compare the +50% with the +100% experiments, then we note the additional +50% SST anomaly added in the +100% case relative to the +50% case is the same anomaly as for the +50% experiment, but added to a warmer background. The response, however, is increased by more than the doubling of the SST anomaly, thus suggesting that the atmospheric response is amplified by a warmer background state. The same holds for all other comparisons. However, some regions do not quite follow this simple principle. The tropical Indian Ocean response to the CP forcing, for instance, is not just increasing with the warming of the SST. In general, the CP pattern does not show as clear an increase in response as the EP pattern.

Figure 10 shows the precipitation response to different strengths and signs of forcings. As expected, the rainfall response in the tropical Pacific is highly nonlinear. For both EP and CP events the relatively weakest response is found for the negative 200% experiments and the strongest for the positive 200% experiments. The nonlinearities are mostly stronger for positive than for negative forcings and stronger over regions with increasing precipitation than decreasing precipitation. Also the response to EP events is more nonlinear than for CP events. A remarkable nonlinearity is seen in the precipitation response over northern Africa and the Arabian Peninsula for both the EP and CP forcing. Here, it changes sign in the normalized response pattern from negative to positive, which means that the precipitation response is the same for El Niño as for La Niña events. There are no indications of this nonlinearity in the observed precipitation response, but the observed SLP response does show some weak indication of such a nonlinearity.

The analysis of Figs. 9 and 10 clearly shows that for both SLP and precipitation the responses more strongly depend on the absolute SSTs than on the SST anomalies, which may be related to the SST threshold for deep convection (Gadgil et al. 1984).

d. Combined effects

In the above analysis sections we concluded that different grades of nonlinearity are found in different regions. To get a better understanding of the different effects of the patterns, strengths, and signs of ENSO events we now focus on a number of different regions: the tropical east Pacific (TEP; 20°S–10°N, 75°–110°W), the tropical west Pacific (TWP; 15°S–15°N, 120°–170°E), the North Pacific (NP; 35°–60°N, 135°W–180°), and the tropical Indian Ocean (TIO; 20°S–10°N, 60°–110°E). Since the nonlinearities in the precipitation response in the tropical Pacific are somewhat expected, and the responses outside the tropical Pacific are of limited confidence, we are focusing on the SLP response in the following section and analyze this in more detail. See Fig. 11 for the SLP response to the EP, CP, and a realistic combined forcing. The realistic combined forcing is a linear combination of the EP and CP forcings and represents what is most closely matching the observed. Dommenget et al. (2013) show that strong positive ENSO events in general have an EP pattern whereas strong negative events have a CP pattern and vice versa for weak events (see also section 2 and Fig. 2). Therefore, in the response to "realistic combined forcings" we combine the responses for 200% CP−, 50% EP− forcing, 50% CP+ forcing, and 200% EP+ forcing and assume that the 100% events can be either EP or CP forcing and thus take their average responses. To quantify the linearity or nonlinearity of the responses, we fitted a linear and a quadratic curve to the data points represented by the mean responses.

In the TEP region the response to either an EP or a CP forcing is linear (Figs. 11a,b). In the TWP the response is nonlinear for both forcing patterns with a slightly stronger nonlinearity for the EP forcing pattern (Figs. 11d,e). For the NP strong nonlinear responses are found for both forcing patterns (Figs. 11g,h). However, here the spread is also wider. For the TIO the overall responses are small compared to the other regions, but a slightly nonlinear response is found for the CP forcing (Figs. 11j,k). If we combine the different forcing patterns to the realistic forcing, we get a very different picture. Over the TEP, where the response to both forcing patterns is linear, we get an indication of a nonlinear response with the realistic forcings (Fig. 11c). This is due to the difference in strength of the responses to EP and CP patterns. The stronger response to the EP pattern gives a stronger than linear response for the +200% and −50% cases and the weaker CP response gives a weaker than linear response for the −200% and +50% cases. Combined this gives a near-quadratic response function with larger response for strong positive (El Niño) events and weaker response for strong negative (La Niña) events.

The opposite is true for the NP region. Both the EP and the CP forcings show a strong nonlinearity. However, in the realistic forcings the nonlinearities cancel each other and lead to a linear response (Fig. 11i). Again, this
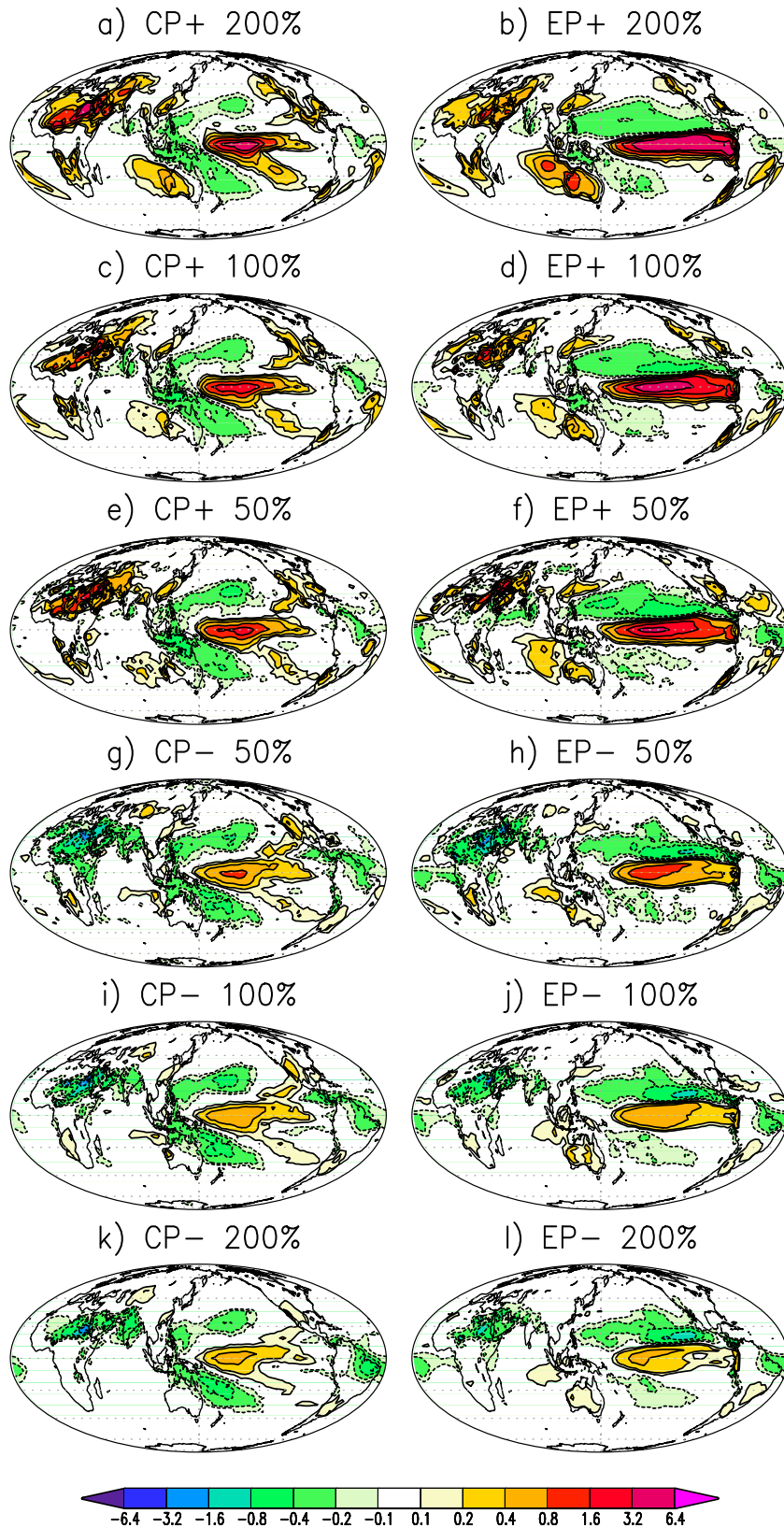
FIG. 10. As in Fig. 9, but for mean precipitation anomalies per climatological precipitation normalized by the Niño-3.4 SST anomalies (% K^{-1}).
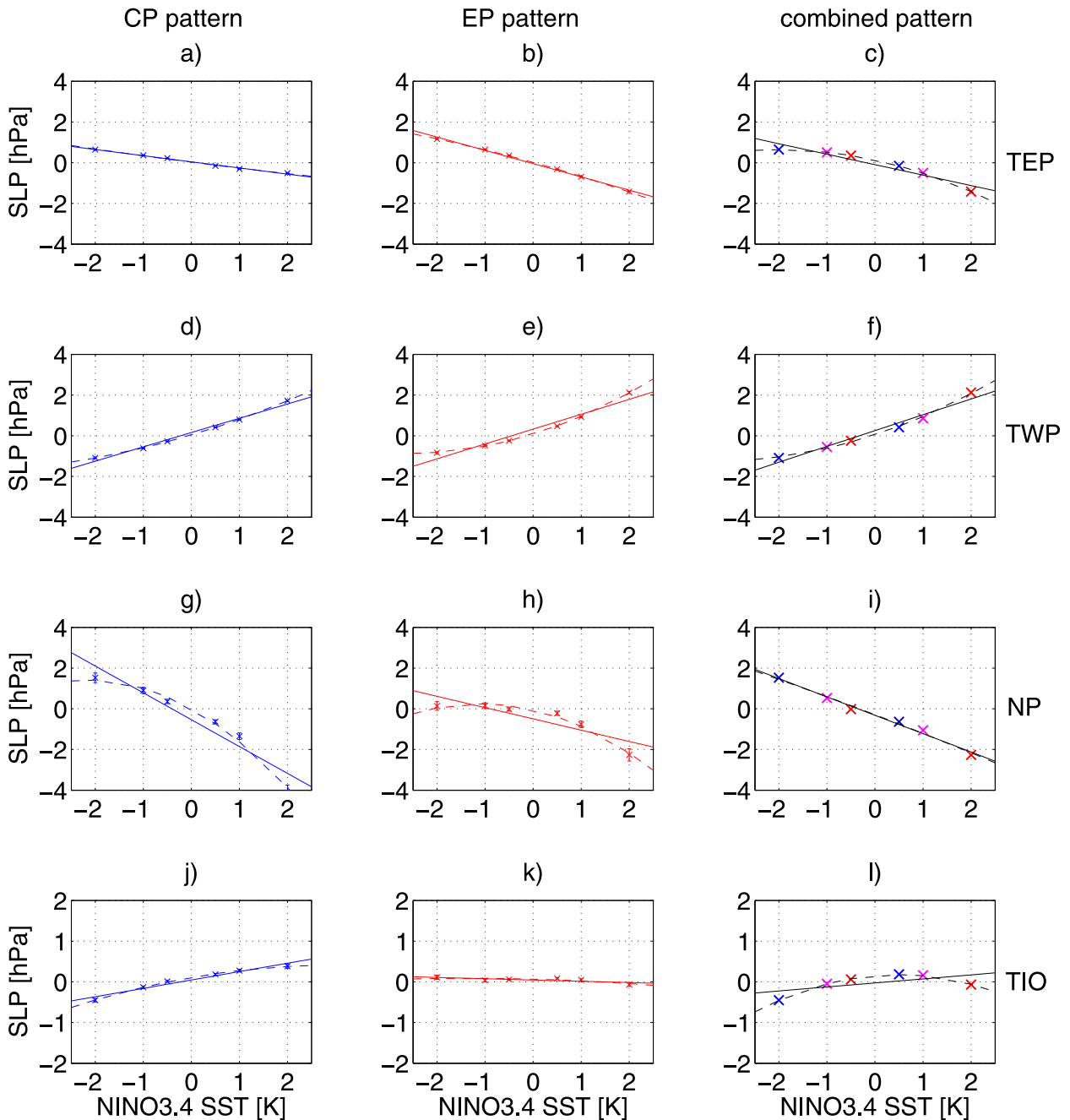
FIG. 11. Summarized SLP responses to CP forcings (blue), EP forcings (red), and combined forcings (black) for the (a)–(c) tropical east Pacific, (d)–(f) tropical west Pacific, (g)–(i) North Pacific, and (j)–(l) tropical Indian Ocean. The crosses indicate the mean SLP response, the error bars indicate one standard error, the dashed lines represent a linear fit, and the solid lines a quadratic fit. For the combined forcings at right the color of the crosses indicates the type of forcing (blue for CP forcing, red for EP forcing, and magenta for CP and EP forcing).

is due to the difference in strength of the responses to the EP and CP patterns, which, when combined, lead to a linear response. In the TIO region the combined response is a significant nonlinear response, which even reverses sign, leading to negative SLP responses for both El Niño and La Niña events (Fig. 11). Again, this is a combination

of a weak response to the EP pattern and a strong response to the CP pattern. In the TWP region all responses are similarly weakly nonlinear, no matter whether we consider EP, CP, or the combination.

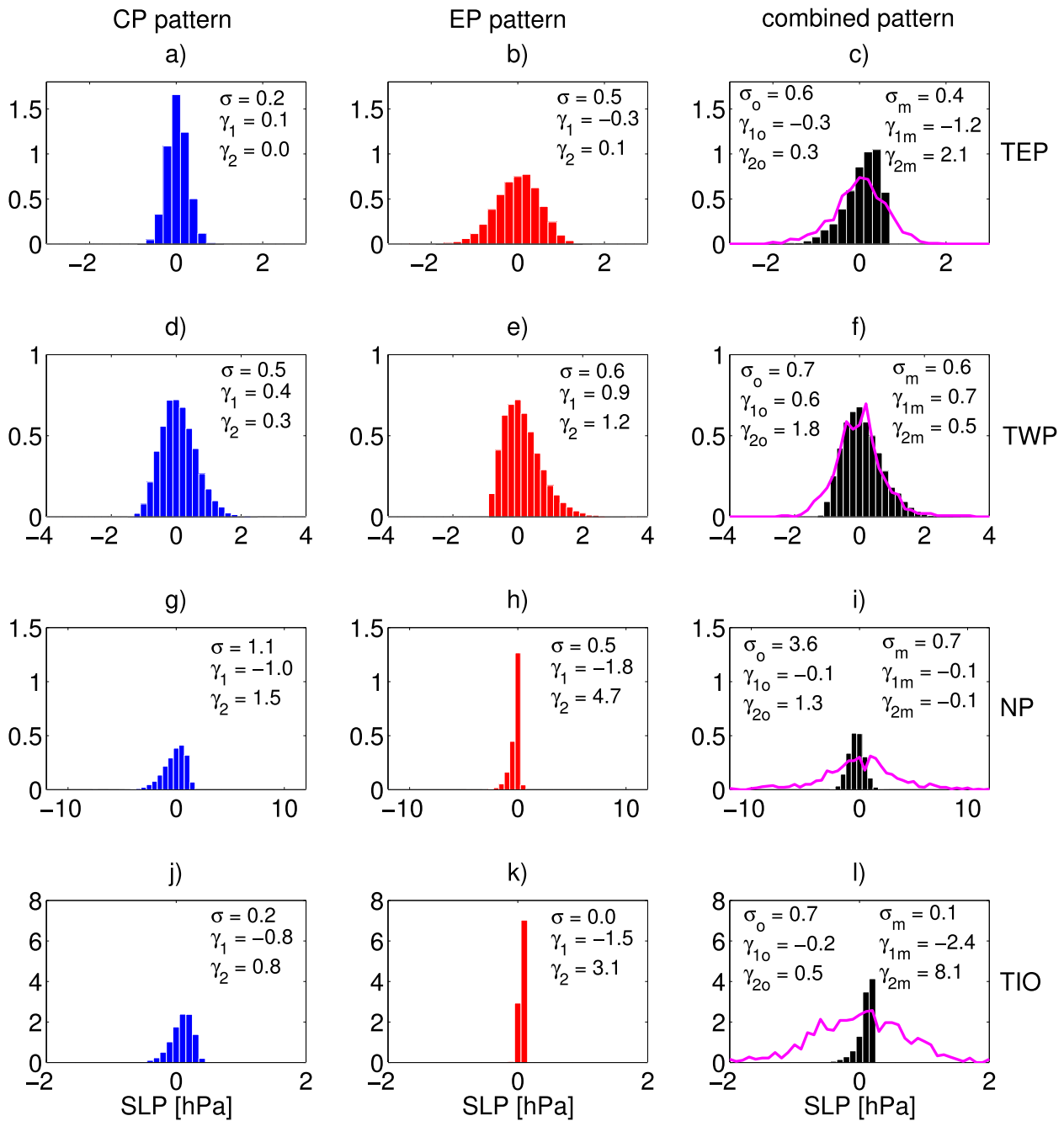Another way to visualize the nonlinearity is to look at histograms of SLP responses over Niño-3.4 SST

FIG. 12. Histograms of SLP responses to 10 000 normally distributed Niño-3.4 SST anomalies with the observed Niño-3.4 SST standard deviation assuming the quadratic relationships as seen in Fig. 11 for CP forcings (blue), EP forcings (red), and combined forcings (black) for the (a)–(c) tropical east Pacific, (d)–(f) tropical west Pacific, (g)–(i) North Pacific, and (j)–(l) tropical Indian Ocean. The bin width is 0.2 K for (a)–(f), 0.5 K for (g)–(i), and 0.1 K for (j)–(l). The magenta curves at right indicate the observed distribution. The observed distributions in (i) and (l) are scaled with the factors 2 and 4, respectively.

anomalies using the fitted quadratic response functions shown in Fig. 11. Therefore, we drew normally distributed random Niño-3.4 SST anomalies (10^4) with the observed Niño-3.4 SST standard deviation and calculated the SLP responses according to the quadratic fits described above.

The resulting SLP histograms with the standard deviation, skewness, and kurtosis can be seen in Fig. 12.

In all four regions the SLP variability in response to the combined CP and EP forcings is less than the observed variability. However, in the TWP and TEP

regions a significant part of the total SLP variability can be attributed to the response to SST variability. Especially in the TWP region this simple model reproduces the observed variability and nonlinearity in the SLP distribution quite well. This, first of all, illustrates that the SLP response to the SST anomalies is a significant part of the total SLP variability in this region. In the TEP region, however, the simple model overestimates the skewness. In the NP and TIO regions the ENSO model-related SLP distributions are much narrower than the observed, which illustrates that the observed SLP variability is not dominated by the ENSO response.

So far, we have only looked at the mean response in four specific regions. However, it is interesting to look at a global distribution of ENSO SLP response nonlinearity. Therefore, we calculated the mean response and its spread for each point and performed the same linear and quadratic fits as above for each point. Figure 13 shows the estimated t values for the CP, EP, and the combined SLP response for deviations from a linear response model. For all three forcings the t values for the quadratic fits are very small (not shown) while the t values for the linear fit are quite significant in several regions, indicating strong nonlinearities. For a CP forcing only weak nonlinearities are found in most of the Pacific basin. The strongest nonlinearity is found over the far western tropical Pacific. Also, in the eastern North Pacific and tropical Pacific north of the equator nonlinearities are found. Nonlinearities are also found over South America and the whole tropical Atlantic. However, there the response itself was very small. For the EP forcing the nonlinearity in the Pacific basin is much stronger. Again, the strongest nonlinearity is found over the western tropical Pacific and the Maritime Continent. Also, in the North Pacific, the eastern tropical Pacific north and south of the equator, the tropical continents, and the tropical Atlantic nonlinearities are found. If we combine the different forcings to the realistic forcings we find the strongest nonlinearities. We find strong nonlinearities over the central to western tropical Pacific and the far eastern tropical Pacific. Also, nonlinearities are found over Central America, the tropical Atlantic, central to southern Africa, the Indian Ocean, and the South Pacific. Again, we also find that the combined realistic response has a near-linear response in the northern North Pacific in contrast to the EP and CP forcing, which are both nonlinear.

5. Summary and discussion

In the study presented here we analyzed the nonlinearity in the ENSO teleconnections based on observations and model simulations. We were interested not only in the differences between strong El Niño and La Niña events but also in the influences of the different factors of pattern, strength, and sign of the SST forcing. Therefore, we performed idealized model experiments in which we forced a full complexity atmospheric GCM with standardized ENSO patterns of different signs and strengths. Our analysis focused on annual mean responses and did not consider seasonal differences. This, however, only reflects the limited space available. Considerable seasonal differences do exist in the characteristics discussed in this analysis, but are left for later studies.

Although the observational database for composites of strong El Niño and La Niña events is very small, we can see that there are significant nonlinearities in the SLP and precipitation responses. The model simulations reproduce the SLP and precipitation response patterns quite well, especially over the Pacific Ocean.

The SLP response shows strong nonlinearities in the tropical Pacific and throughout the whole tropics and subtropics. In most regions the main characteristic of the SLP response per unit SST anomaly is that it is stronger for warmer SST anomalies. This is similar to the nonlinearities found in the zonal wind and SST interactions in the tropical Pacific (e.g., Kang and Kug 2002; Philip and van Oldenborgh 2009; Frauen and Dommenget 2010; Dommenget et al. 2013) and the nonlinearities found by Bayr et al. (2014) in the Walker circulation response. In the literature so far there has been no physical explanation given for why we see a stronger atmospheric circulation response for warmer SST anomalies of ENSO. However, it is plausible to assume that this is related to the nonlinearities associated with the moist convection intensities. These are to a large part controlled by the Clausius–Clapeyron relationship, which allows for stronger atmospheric circulation responses for warmer SSTs due to nonlinear increases in saturated water vapor levels. However, it is beyond this study to support this link in physical processes.

The nonlinearities in precipitation are mostly confined to the tropical Pacific and for the most part follow from the basic nonlinearities that we see for the precipitation distributions in general. The shifts that we find in the tropical Pacific are consistent with those found by Chung et al. (2014) and Power et al. (2013).

Studying the combined influence of the pattern, strength, and the sign of the event shows that each component plays a role for the nonlinearities. For SLP it can be seen that the nonlinearity is stronger for an EP forcing pattern than for a CP forcing pattern. If we take into account that strong positive events generally have an EP pattern and strong negative events a CP pattern (and vice versa for weak events) and combine the responses accordingly, we find overall the strongest nonlinearities. However, this has different effects over different regions.

a) CP pattern
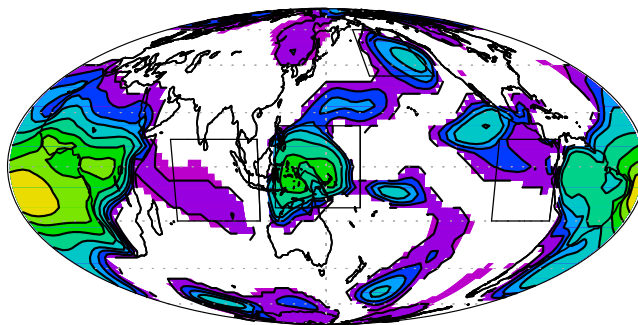
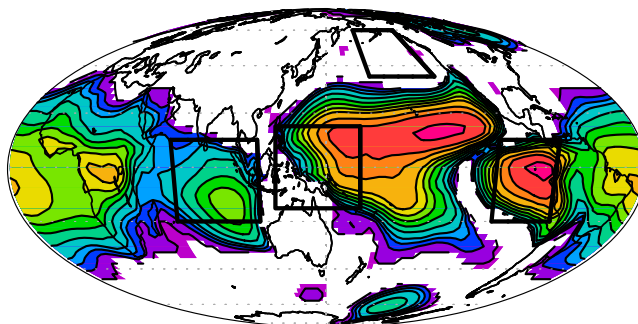## b) EP pattern
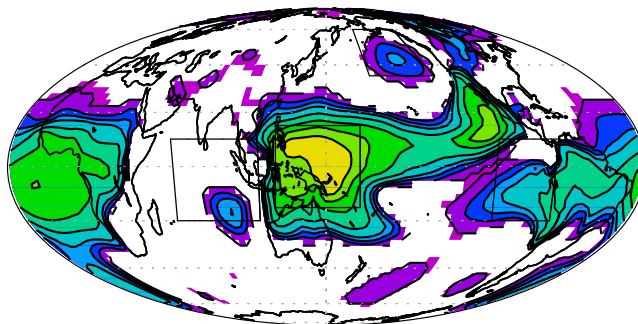
c) combined

FIG. 13. Estimated *t* values for the deviations of the SLP responses from a linear fit (dashed lines in Fig. 11) for (a) CP forcings, (b) EP forcings, and (c) combined forcings.

Over regions like the far eastern tropical Pacific the response to each forcing pattern separately is mostly linear. When we combine the forcings realistically, we find a strong nonlinearity. The opposite is true for the North Pacific, where the response to each pattern separately is nonlinear. In the realistic combination of the responses, however, the nonlinearities cancel each other and the response is linear.

The nonlinearities particularly in the tropics are of considerable magnitude. In some regions they can be larger than the linear response (e.g., tropical Indian Ocean or central equatorial Pacific). This suggests that models based on linear assumptions will perform much worse in predicting the right teleconnections in some regions than models considering the right nonlinearities. They may even predict the wrong sign of the response.

Since much of this nonlinearity suggests a mean state dependence (warmer mean SST leading to stronger responses), the result also suggests that correct mean states are essential in predicting the correct ENSO teleconnections.

Also, in order for both climate models and dynamical seasonal prediction models to realistically simulate and predict ENSO teleconnections it is important to realistically simulate not only the amplitude of events but also the different patterns of events. However, state-of-the-art seasonal prediction models, such as the European Centre for Medium-Range Weather Forecasts (ECMWF) Seasonal Forecast System 4 and NCEP Climate Forecast System (CFS) version 2, have too strong ENSO variability and the peak of the variability too far east (Kim et al. 2012). Also, current models are not capable in simulating realistic ENSO diversity in the EP and CP events (Ham and Kug 2012; Yang and Jiang 2014) and basically all models have substantial mean state biases, which will affect the nonlinear aspects of the teleconnections (Bellenger et al. 2014).

The main conclusion of our work is that the linearity or nonlinearity of ENSO teleconnections results from a combination of two effects: a linear response to a spatially nonlinear ENSO (varying ENSO patterns) and a nonlinear response to a linear ENSO (fixed patterns but varying signs and strengths). For the analysis of ENSO teleconnections, especially also in fully coupled GCMs and future climate projections, it is not sufficient to build response models based on linear regression or composites based only on the sign of events. The observed differences between strong El Niño and La Niña events are in general a combination of both of these effects. In the tropical Pacific region the effects of the different patterns are dominant, shifting a mostly linear response of the atmosphere following the position of the maximum SST anomalies. In remote tropical regions and in particular in the extratropical regions the combination of both effects is relevant. However, given the limitations of the model used in this study we cannot attribute all differences in the ENSO events to nonlinear dynamics. Some aspects, particular in remote regions, are still unclear and some aspects may simply be random sampling effects.

REFERENCES

Adler, R. F., and Coauthors, 2003: The Version-2 Global Precipitation Climatology Project (GPCP) monthly precipitation analysis (1979–present). *J. Hydrometeor.,* **4,** 1147–1167, doi:10.1175/1525-7541(2003)004<1147:TVGPCP>2.0.CO;2.

An, S.-I., and F.-F. Jin, 2004: Nonlinearity and asymmetry of ENSO. *J. Climate,* **17,** 2399–2412, doi:10.1175/1520-0442(2004)017<2399:NAAOE>2.0.CO;2.

Ashok, K., S. K. Behera, S. A. Rao, H. Y. Weng, and T. Yamagata, 2007: El Niño Modoki and its possible teleconnection. *J. Geophys. Res.,* **112,** C11007, doi:10.1029/2006JC003798.

Bayr, T., D. Dommenget, T. Martin, and S. Power, 2014: The eastward shift of the Walker circulation in response to global warming and its relationship to ENSO variability. *Climate Dyn.,* doi:10.1007/s00382-014-2091-y, in press.

Bellenger, H., E. Guilyardi, J. Leloup, M. Lengaigne, and J. Vialard, 2014: ENSO representation in climate models: From CMIP3 to CMIP5. *Climate Dyn.,* **42,** 1999–2018, doi:10.1007/s00382-013-1783-z.

Bi, D., and Coauthors, 2013: The ACCESS coupled model: Description, control climate and evaluation. *Aust. Meteor. Oceanogr. J.,* **63,** 41–64.

Burgers, G., and D. B. Stephenson, 1999: The "normality'' of El Niño. *Geophys. Res. Lett.,* **26,** 1027–1030, doi:10.1029/1999GL900161.

Cai, W., P. van Rensch, T. Cowan, and A. Sullivan, 2010: Asymmetry in ENSO teleconnection with regional rainfall, its multidecadal variability, and impact. *J. Climate,* **23,** 4944–4955, doi:10.1175/2010JCLI3501.1.

Choi, J., S.-I. An, and S.-W. Yeh, 2012: Decadal amplitude modulation of two types of ENSO and its relationship with the mean state. *Climate Dyn.,* **38,** 2631–2644, doi:10.1007/s00382-011-1186-y.

Chung, C., S. Power, J. Arblaster, H. Rashid, and G. Roff, 2014: Nonlinear precipitation response to El Niño and global warming in the Indo-Pacific. *Climate Dyn.,* **42,** 1837–1856, doi:10.1007/s00382-013-1892-8.

Davies, T., M. J. P. Cullen, A. J. Malcolm, M. H. Mawson, A. Staniforth, A. A. White, and N. Wood, 2005: A new dynamical core for the Met Office's global and regional modelling of the atmosphere. *Quart. J. Roy. Meteor. Soc.,* **131,** 1759–1782, doi:10.1256/qj.04.101.

Dommenget, D., 2010: The slab ocean El Niño. *Geophys. Res. Lett.,* **37,** L20701, doi:10.1029/2010GL044888.

——, and M. Latif, 2002: Analysis of observed and simulated SST spectra in the midlatitudes. *Climate Dyn.,* **19,** 277–288, doi:10.1007/s00382-002-0229-9.

——, T. Bayr, and C. Frauen, 2013: Analysis of the non-linearity in the pattern and time evolution of El Niño Southern Oscillation. *Climate Dyn.,* **40,** 2825–2847, doi:10.1007/s00382-012-1475-0.

Enfield, D. B., and D. A. Mayer, 1997: Tropical Atlantic sea surface temperature variability and its relation to El Niño–Southern Oscillation. *J. Geophys. Res.,* **102,** 929–945, doi:10.1029/96JC03296.

Frauen, C., and D. Dommenget, 2010: El Niño and La Niña amplitude asymmetry caused by atmospheric feedbacks. *Geophys. Res. Lett.,* **37,** L18801, doi:10.1029/2010GL044444.

Gadgil, S., P. V. Joseph, and N. V. Joshi, 1984: Ocean–atmosphere coupling over monsoon regions. *Nature,* **312,** 141–143, doi:10.1038/312141a0.

Graf, H.-F., and D. Zanchettin, 2012: Central Pacific El Niño, the subtropical bridge, and Eurasian climate. *J. Geophys. Res. Atmos.,* **117,** D01102, doi:10.1029/2011JD016493.

Ham, Y.-G., and J.-S. Kug, 2012: How well do current climate models simulate two types of El Niño? *Climate Dyn.,* **39,** 383–398, doi:10.1007/s00382-011-1157-3.

Hoerling, M. P., A. Kumar, and M. Zhong, 1997: El Niño, La Niña, and the nonlinearity of their teleconnections. *J. Climate,* **10,** 1769–1786, doi:10.1175/1520-0442(1997)010<1769:ENOLNA>2.0.CO;2.

——, ——, and T. Y. Xu, 2001: Robustness of the nonlinear climate response to ENSO's extreme phases. *J. Climate,* **14,** 1277–1293, doi:10.1175/1520-0442(2001)014<1277:ROTNCR>2.0.CO;2.

Hu, Z.-Z., A. Kumar, B. Jha, W. Wang, B. Huang, and B. Huang, 2012: An analysis of warm pool and cold tongue El Niños: Air–sea coupling processes, global influences, and recent trends. *Climate Dyn.,* **38,** 2017–2035, doi:10.1007/s00382-011-1224-9.

Kalnay, E., and Coauthors, 1996: The NCEP/NCAR 40-Year Reanalysis Project. *Bull. Amer. Meteor. Soc.,* **77,** 437–471, doi:10.1175/1520-0477(1996)077<0437:TNYRP>2.0.CO;2.

Kang, I.-S., and J.-S. Kug, 2002: El Niño and La Niña sea surface temperature anomalies: Asymmetry characteristics associated with their wind stress anomalies. *J. Geophys. Res.,* **107,** 4372, doi:10.1029/2001JD000393.

Kim, H.-M., P. J. Webster, and J. A. Curry, 2012: Seasonal prediction skill of ECMWF System 4 and NCEP CFSv2 retrospective forecast for the Northern Hemisphere winter. *Climate Dyn.,* **39,** 2957–2973, doi:10.1007/s00382-012-1364-6.

Larkin, N. K., and D. E. Harrison, 2002: ENSO warm (El Niño) and cold (La Niña) event life cycles: Ocean surface anomaly patterns, their symmetries, asymmetries, and implications. *J. Climate,* **15,** 1118–1140, doi:10.1175/1520-0442(2002)015<1118:EWENOA>2.0.CO;2.

Latif, M., and T. P. Barnett, 1995: Interactions of the tropical oceans. *J. Climate,* **8,** 952–964, doi:10.1175/1520-0442(1995)008<0952:IOTTO>2.0.CO;2.

Lin, J.-L., 2007: The double-ITCZ problem in IPCC AR4 coupled GCMs: Ocean–atmosphere feedback analysis. *J. Climate,* **20,** 4497–4525, doi:10.1175/JCLI4272.1.

Martin, G. M., S. F. Milton, C. A. Senior, M. E. Brooks, S. Ineson, T. Reichler, and J. Kim, 2010: Analysis and reduction of systematic errors through a seamless approach to modeling weather and climate. *J. Climate,* **23,** 5933–5957, doi:10.1175/2010JCLI3541.1.

——, and Coauthors, 2011: The HadGEM2 family of Met Office Unified Model climate configurations. *Geosci. Model Dev.,* **4,** 723–757, doi:10.5194/gmd-4-723-2011.

Murphy, J. M., D. M. H. Sexton, D. N. Barnett, G. S. Jones, M. J. Webb, M. Collins, and D. A. Stainforth, 2004: Quantification of modelling uncertainties in a large ensemble of climate change simulations. *Nature,* **430,** 768–772, doi:10.1038/nature02771.

Ohba, M., and H. Ueda, 2009: Role of nonlinear atmospheric response to SST on the asymmetric transition process of ENSO. *J. Climate,* **22,** 177–192, doi:10.1175/2008JCLI2334.1.

Okumura, Y. M., and C. Deser, 2010: Asymmetry in the duration of El Niño and La Niña. *J. Climate,* **23,** 5826–5843, doi:10.1175/2010JCLI3592.1.

Philip, S., and G. J. van Oldenborgh, 2009: Significant atmospheric nonlinearities in the ENSO cycle. *J. Climate,* **22,** 4014–4028, doi:10.1175/2009JCLI2716.1.

Power, S., M. Haylock, R. Colman, and X. Wang, 2006: The predictability of interdecadal changes in ENSO activity and ENSO teleconnections. *J. Climate,* **19,** 4755–4771, doi:10.1175/JCLI3868.1.

——, F. Delage, C. Chung, G. Kociuba, and K. Keay, 2013: Robust twenty-first-century projections of El Niño and related precipitation variability. *Nature,* **502,** 541–545, doi:10.1038/nature12580.

Rayner, N. A., D. E. Parker, E. B. Horton, C. K. Folland, L. V. Alexander, D. P. Rowell, E. C. Kent, and A. Kaplan, 2003: Global analyses of sea surface temperature, sea ice, and night marine air temperature since the late nineteenth century. *J. Geophys. Res.,* **108,** 4407, doi:10.1029/2002JD002670.

Smith, I., A. Moise, K. Inape, B. Murphy, R. Colman, S. Power, and C. Chung, 2013: ENSO-related rainfall changes over the New Guinea region. *J. Geophys. Res. Atmos.,* **118,** 10 665–10 675, doi:10.1002/jgrd.50818.

Takahashi, K., A. Montecinos, K. Goubanova, and B. Dewitte, 2011: ENSO regimes: Reinterpreting the canonical and Modoki El Niño. *Geophys. Res. Lett.,* **38,** L10704, doi:10.1029/2011GL047364.

Taschetto, A. S., and M. H. England, 2009: El Niño Modoki impacts on Australian rainfall. *J. Climate,* **22,** 3167–3174, doi:10.1175/2008JCLI2589.1.

Washington, W. M., and G. A. Meehl, 1984: Seasonal cycle experiment on the climate sensitivity due to a doubling of CO_2 with an atmospheric general circulation model coupled to a simple mixed-layer ocean model. *J. Geophys. Res.,* **89,** 9475–9503, doi:10.1029/JD089iD06p09475.

Yang, S., and X. Jiang, 2014: Prediction of eastern and central Pacific ENSO events and their impacts on East Asian climate by the NCEP Climate Forecast System. *J. Climate,* **27,** 4451–4472, doi:10.1175/JCLI-D-13-00471.1.

Yu, J.-Y., and S. T. Kim, 2011: Reversed spatial asymmetries between El Niño and La Niña and their linkage to decadal ENSO modulation in CMIP3 models. *J. Climate,* **24,** 5423–5434, doi:10.1175/JCLI-D-11-00024.1.

Yuan, Y., and S. Yang, 2012: Impacts of different types of El Niño on the East Asian climate: Focus on ENSO cycles. *J. Climate,* **25,** 7702–7722, doi:10.1175/JCLI-D-11-00576.1.

Zhang, W. J., F.-F. Jin, H.-L. Ren, J. Li, and J.-X. Zhao, 2012: Differences in teleconnection over the North Pacific and rainfall shift over the USA associated with two types of El Niño during boreal autumn. *J. Meteor. Soc. Japan,* **90,** 535–552, doi:10.2151/jmsj.2012-407.